RESEARCH ARTICLE

No-Load Characteristic Analysis of Single/Three-Phase Dual-Port Permanent Magnet Synchronous Generator With Eccentric Magnetic Metal Block Based on Nonlinear Magnetic Field Analytical Method

KAI LI[ID], BINGYI ZHANG, GUIHONG FENG, AND KAI LIU

School of Electrical Engineering, Shenyang University of Technology, Shenyang 110870, China

Corresponding author: Guihong Feng (fenggh@sut.edu.cn)

ABSTRACT The establishment of no-load magnetic field model is of great significance to the optimization design and performance analysis of permanent magnet synchronous generator (PMSG). The authors describe the basic structure and operating principle of the single/three-phase dual-port permanent magnet synchronous generator (STPDP-PMSG), and optimizes the dimension parameters of the surface-mounted magnetic pole consisting of magnetic metal block and permanent magnet to obtain an optimal rotor pole structure parameter. Considering the nonlinear variation of the stator and rotor core permeability, based on the analytical method of nonlinear subdomain model, the magnetic field model of STPDP-PMSG is established to analyze its no-load characteristics. Furthermore, the authors calculate and analyze the no-load air gap flux density and no-load back electromotive force (BEMF) of the generator, and the finite element method is used for verification. Finally, an experiment is conducted on a 4-pole 48-slot STPDP-PMSG with eccentric magnetic metal block. The measured no-load BEMF is basically consistent with the analytical calculation value, which verifies the accuracy of the nonlinear subdomain model proposed in this study.

INDEX TERMS STPDP-PMSG, optimize, no-load characteristics, nonlinear subdomain model.

I. INTRODUCTION

Oil, coal mines and other industries that require field operation vehicles, single-phase loads such as field lighting and testing equipment have an increasing demand for single-phase power supplies. If a three-phase generator is used to drive three-phase load and single-phase load at the same time to meet the requirements of the single-phase load on the working site, the power redundancy of the three-phase generator will be large, which will increase the unbalance degree of the three-phase port of traditional three-phase generator. If the single-phase power generation system is separately equipped for single-phase load, the volume and weight of the power generation system will also be increased.

The associate editor coordinating the review of this manuscript and approving it for publication was Paolo Giangrande[ID].

To reduce the volume and weight of power on-board generation system, the authors designed a STPDP-PMSG with stator slot of varied depth, as shown in Fig. 1. The stator structure consists of a set of three-phase windings to output three-phase alternating current and a set of single-phase windings to output single-phase alternating current. The two sets of stator windings are electrically and mechanically independent of each other and only coupling on the magnetic circuit. The rotor structure is composed of rectangular magnetic steel and conducted magnetic metal block with eccentric outer arc.

STPDP-PMSG is a new type of generator with a three-phase alternating current (AC) port, a single-phase AC port and a public mechanical port. This type of generator solves the above problems happening in the field operation of the traditional field vehicle's on-board power generation

system. At the same time, it also solves a series of problems such as large area, low reliability, high maintenance cost and low power density of multiple power generation equipment. It has the advantages of high power density, high reliability, low maintenance cost and small size. However, affected by its single stator double winding structure, the saturation state of the core and the single-phase pulse magneto-motive force in the air gap magnetic field during the operation, STPDP-PMSG exhibits a high degree of non-linearity. The accurate calculation of the magnetic field distribution in the air gap of STPDP-PMSG is the key to designing and optimizing its electromagnetic performance. The commonly used finite element method (FEM) can effectively handle complex models with high calculation accuracy, but its calculation time is relatively long. While the analytical method (ANA) has faster calculation speed, smaller calculation amount and clearer physical concept, which is conducive to the design and optimization of the initial scheme of STPDP-PMSG. In [1], [2], [3], and [4], Analytical calculation methods mainly include equivalent magnet circuit network (EMCN) method, subdomain model method and harmonic modeling method. The subdomain model method is currently the most commonly used method for analytic modeling of the magnetic field of the generator. It is mainly based on the method of separation of variables to obtain the Fourier series form solution of each subdomain. The calculation accuracy of this method is also higher in comparison with the FEM results, which is proven in [5] and [6].

Because the stator slotting can lead to the distortion of the air gap flux density and the increase of harmonic components, it is difficult to accurately calculate the air gap flux of STPDP-PMSG based on the analytical method. In [7], the maximum value of air gap flux considering slot effect can be obtained by using traditional magnetic circuit method corrected by empirical coefficient. However, if the stator shape and parameters of STPDP-PMSG are irregular, the empirical correction coefficient is difficult to obtain, which makes the calculation accuracy of traditional magnetic circuit method considering slotting effect not high. The subdomain method divides the irregular region of the motor into different regular regions to solve the problem, and establishes the relation of the Laplace equation or Poisson equation of each subdomain through the interface condition. Then the distribution of the air gap magnetic field can be obtained by using the analytic results of the subdomain method [9], [10].

Many scholars have done a lot of research on the analytical models of different motor structures, as shown in Table 1. Reference [11]establish an accurate subdomain model of the rotor eccentric structure of slotless surface-mount permanent magnet motors, which reduce the harmonic content of air gap flux density under rotor eccentricity conditions. Reference [12] perform an analytical calculation of the magnetic field of surface-mount PMG with eccentric rotor, then calculates the air gap flux density and cogging torque, research has shown that changing the eccentric distance of the pole can greatly

TABLE 1. Magnetic field analysis method of different structure machines.

Author	Method	Machine structure
Z. J Qiu, et al. (2013) [11]	a static eccentric analytical model based on the boundary perturbation method	Surface-Mounted PMSM
Y. Zhou, H. et al. (2015) [12]	surface current method of permanent magnet, subdomain model and superposition principle of vector potential.	Conventional Surface-Mounted PMSM
M. Baghayipour, et al. (2018) [13]	an analytical model considering the iron saturation and winding distribution	Conventional Axial Flux PM machines
S. S. Zhang, et al. (2019) [14]	accurate subdomain model considering the periodic boundary condition	Conventional Surface-Mounted PMSM
LI Chen, et al. (2013) [15]	two-dimensional exact analytical method	Conventional Halbach-array PMSM
T. Y. Guo, et al. (2015) [16]	accurate subdomain model	Conventional Surface-Inset PMSM
H. C. Li, et al. (2017) [17]	subdomain model under the condition of neglecting magnetic saturation	Surface-Mounted PMSM

reduce the harmonic content of radial flux density, and the cogging torque can be reduced at the same time [13]. An analytical model for the harmonic content no-load magnetic fields and BEMF in TORUS-NS AFPM machines with surface mounted magnets considering the winding distribution and iron saturation effects is proposed. This method yields the no-load magnetic field distributions in air-gap and iron cores and BEMF very exactly. Reference [14] establish a magnetic field analytical calculation model of the surface-mounted PMSM, and consider the effects of the step skewing of permanent magnet and magnetic slot wedge. In [15] and [16], the authors establish an accurate subdomain model of the half-open slot of the surface-mounted PMSM with Halbach structure, and verifies it through finite element analysis and experiments. In [17], the authors establish the accurate subdomain analytical model of the permanent magnet machines with a surface-inset rotor structure, and calculates the distribution of no-load magnetic field, armature magnetic field and load magnetic field of the motor. In [18], the authors use the irregular yoke radius function and the eccentric permanent magnet radius function to solve the no-load air gap magnetic field, and analytically derives the no-load air gap magnetic field of the polygonal rotor yoke PMSM. Compared with the finite element simulation analysis, the two calculation results are in good agreement. The above method can accurately simulate the magnetic field analytical calculation of the motors with different structures, however, the length of the air gap may change with the constant change of rotor eccentric distance, but there is no specific solution to this problem, which has certain limitations, and the single/three-phase dual-port structure is not mentioned.
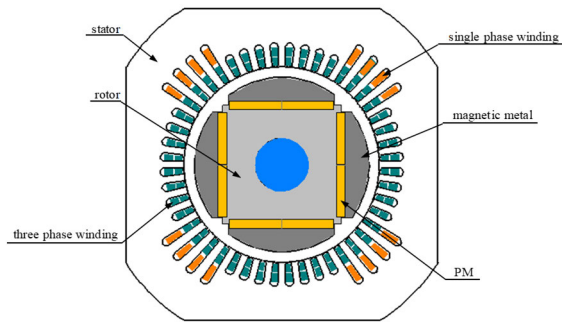
FIGURE 1. The structure of STPDP-PMSG.

FIGURE 2. The operating principle of STPDP-PMSG.

As shown in Table 1, different analytical methods can be used to establish magnetic field models for motors with different structures and obtain good experimental results. Besides, the no-load characteristics of this new structure generator has not been discussed in the published literature. On the basis of previous studies, the authors take a STPDP-PMSG with eccentric magnetic metal block as the research object. The stator structure of this study adopts two sets of windings, which can supply power to three-phase load and single-phase load simultaneously. Rectangular magnetic steel and magnetic metal block constitute the surface-mounted pole structure of STPDP-PMSG.

To analyze this particular structure in detail, the STPDP-PMSG nonlinear subdomain model considering the nonlinear variation of stator permeability and rotor core permeability is established on the two-dimensional polar coordinate plane. The authors optimize the size parameters of the generator rotor pole, which include the pole arc coefficient of the magnetic pole and the eccentric distance of the magnetic metal block, obtain the optimal rotor pole structural parameters, then reduce the air gap flux density and the harmonic content of no-load BEMF. Finally, the authors design and manufacture a 4-pole 48-slot STPDP-PMSG with eccentric magnetic metal block. The comparison and analysis of finite element simulation results and experimental test results verify the accuracy of the nonlinear subdomain model. The study reveals the correctness of the special structure of STPDP-PMSG, utilizes the space of stator punching, thereby avoiding material waste and improving the power density of the generator, thus providing a reference for subsequent generator design.

II. THE BASIC STRUCTURE AND OPERATING PRINCIPLE OF STPDP-PMSG

STPDP-PMSG is a multi-port generator composed of two electrical ports and one mechanical port. It is composed of a set of three-phase windings and single-phase windings in a stator, and a set of rotors (See Fig. 1). Two sets of three-phase windings and a set of single-phase windings with the same number of pole pairs are respectively embedded on the stator. As shown in Fig.1, the three-phase winding is a double-layer distributed winding, which is distributed in the stator slot along the circumferential direction; the single-phase winding
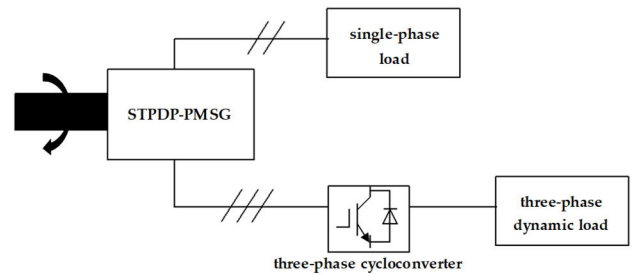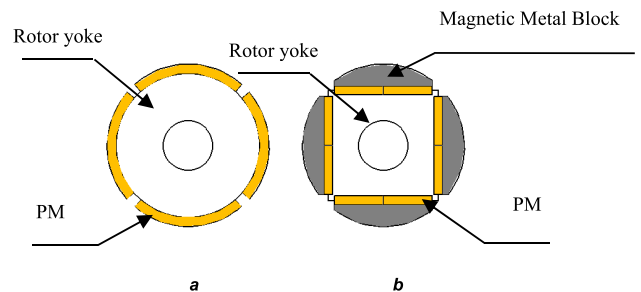

FIGURE 3. Comparison of conventional surface-mounted magnetic pole structure and the new type of surface-mounted magnetic pole structure.

is a single-layer concentric winding, which is located in the upper part of the slot at the four corners of the stator. This structure is more compact, which can effectively reduce the size of the generator. As shown in Figure 2, the three-phase port is connected to a three-phase load and the single-phase port is connected to a single-phase load. The two sets of windings are independently connected to their respective loads and share a rotor magnetic circuit. The two sets of windings share the same stator magnetic circuit and thus they are directly coupled structures.

The conventional surface-mounted magnetic pole structure is shown in Figure 3(a), and the new type of surface-mounted magnetic pole structure in this study is shown in Figure 3(b).

The difference between the two surface-mounted magnetic pole structures is that the permanent magnet in the new structure can be machined according to a simple rectangular structure, and it can be placed in the flat bottom slot milled out of the rotor surface during assembly. The uneven air gap structure can be realized by reasonably designing the eccentric structure shape of the magnetic metal block, and then the purpose of improving the air gap magnetic density waveform can be achieved. In addition, the magnetic metal block can also protect the magnetic steel during rotor assembly. The eddy current loss caused by teeth harmonics is concentrated on the surface of the metal block rather than the surface of the permanent magnet, and the permanent magnet does not have the risk of high temperature demagnetization, therefore, the permanent magnet can be machined in one piece along the axis. Due to the good toughness and easy processing of metal materials, the structure is equipped with countersunk screw holes on the magnetic metal block during assembly. Opening corresponding circular holes on the magnetic steel can fix

TABLE 2. STPDP PMSG parameters.

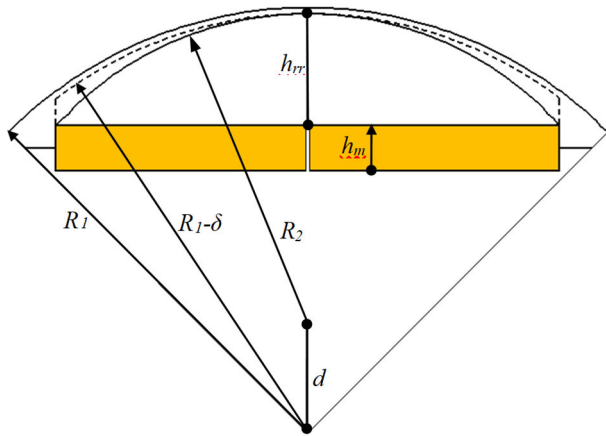| Parameter	Unit	Value
three-phase rated power	kW	80
single-phase rated power	kW	30
stator outer diameter	mm	420
stator inner diameter	mm	299
rotor outer diameter	mm	297
rated speed	r/min	1500
poles		4
slots		48
thickness of PM	mm	16.5

FIGURE 4. Eccentric structure of the magnetic metal block.

it well in the flat bottom slot milled on the rotor surface. Obviously, this structure effectively avoids the problem of high processing scrap rate caused by the complex shape of the magnetic steel structure, and can reduce the processing cost of permanent magnets and the manufacturing cost of the generator to a certain extent.

According to the structural characteristics of STPDP PMSG, the authors design a prototype with three-phase power of 80kW and single-phase power of 30kW. The specific structural parameters are shown in Table 2.

III. ESTABLISHMENT OF ANALYTICAL MODEL OF SURFACE-MOUNTED STPDP-PMSG WITH ECCENTRIC MAGNETIC METAL BLOCK

A. ESTABLISHMENT OF ECCENTRIC STRUCTURE MODEL OF THE MAGNETIC METAL BLOCK OF STPDP-PMSG

Genetic algorithm is a random search algorithm that based on natural selection and genetic mechanism in the biological world, which searches for the optimal solution by simulating the natural evolution process [19], [20]. Considering that randomness can make the solution traverse the whole value space, genetic algorithm is adopted for optimization in this paper.

It can be seen from Figure 4 that there must be an eccentric distance d corresponding to an h_{rr}, which makes the sinusoidal distortion rate of the air gap magnetic density

waveform smallest, the sine degree of the waveform best, and the harmonic content minimum. Therefore, it is necessary to optimize the size of the magnetic pole structure.

According to the geometric diagram of eccentric structure of the rotor pole (See Fig. 4), on the premise of determining the minimum length of the air gap, the authors provide a mathematical expression using genetic optimization algorithm, as shown in (1).

$$\begin{cases} \min f(x) = \dfrac{\sum\limits_{i=2}^{\infty} B_{ri}}{B_1} \times 100\% \\ x = (d, h_{rr}, \alpha_p) \\ s.t. R_2 + (h_m + h_{rr}) \leq R_1 - \delta; 0 \leq d \leq R_2 \end{cases} \quad (1)$$

where B_1 and B_{ri} are the fundamental wave amplitude and harmonic amplitude values of the air gap magnetic density, respectively. Where δ is the air gap length, α_p is the polar arc coefficient of permanent magnet, h_m is the magnetization direction length of permanent magnet, d is the eccentric distance of the rotor outside diameter which determines the outer arc of the magnetic metal block, d is the eccentric distance of the magnetic metal block. h_{rr} is the center thickness of pole, R_1 is the inner radius of stator, R_2 is the outer radius of rotor.

This optimization realizes the uneven air gap structure of the generator by rationally designing the structure and shape of the magnetic metal block, and achieves the purpose of improving the air gap flux density waveform of the generator. Since the pole arc coefficient also has a great impact on the air gap flux density waveform of the generator, to better improve the sine of the waveform, the pole arc coefficient is also considered in the optimization. Therefore, the optimization of the new pole structure size should be a single-objective, multi-variable and constrained geometric shape optimization.

B. OPTIMIZATION OF ECCENTRIC STRUCTURE MODEL OF THE MAGNETIC METAL BLOCK OF STPDP-PMSG

To reduce the distortion rate of the no-load air gap flux density waveform of STPDP-PMSG, the authors use a genetic optimization algorithm based on the analytical method of nonlinear accurate subdomain model to optimize the eccentric structure of the pole in Fig. 4. The optimization variables include the pole arc coefficient of permanent magnet (α_p) and the outer circular eccentric distance of the outer arc of rotor pole (d). Under the premise of determining the minimum air gap length of PMG, the parameterized design of the optimized variables is carried out. Fig. 5 shows the distribution of the distortion rate of air gap flux density waveform under different pole arc coefficients of permanent magnet and the outer circular eccentric distance of the outer arc of rotor pole (d). It can be seen from the figure that the distortion rate first decreases and then increases with the increase of the d. When d is between 4mm and 6mm, the sinusoidal characteristics of the radial air gap flux density waveform is relatively good, and the minimum distortion rate of air gap flux density is 9.1101%.
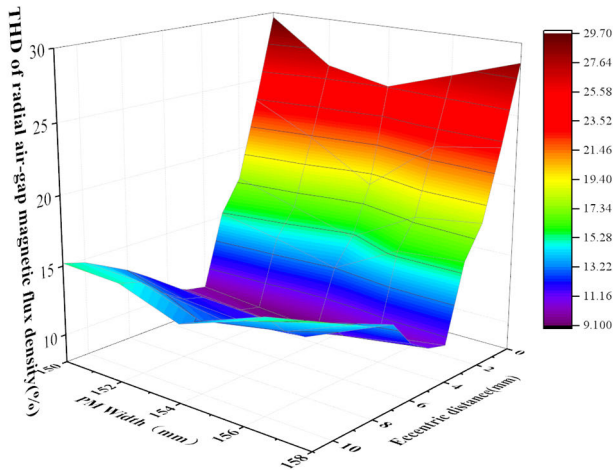
FIGURE 5. Three-dimensional distribution of the distortion rate of radial flux density waveform of STPDP-PMSG.

FIGURE 6. Two-dimensional schematic diagram of STPDP-PMSG.

The influence of the pole arc coefficient on the distortion rate of air gap flux density waveform is complicated. After comprehensive considerations, the authors determine the outer circular eccentric distance of the outer arc of rotor pole (d) is 4mm, and the pole arc coefficient is 0.86.

C. ESTABLISHMENT AND SOLUTION OF STPDP-PMSG NONLINEAR MAGNETIC POTENTIAL EQUATION

The authors take the STPDP-PMSG with the structure in Fig.1 as an example to derive and solve. The two-dimensional schematic diagram of the generator is shown in Fig.6. To facilitate the analysis, the authors make the following basic assumptions:

1) Ignoring the change of the magnetic field in the z-axis direction, the currents only flow in the z-axis direction, which is: $A_z = A(r, \theta)$.
2) The current density is equivalent to the actual value of the stator winding current.
3) Assuming that the conductor load current changes sinusoidally with time.
4) The magnetic The magnetic permeability of the stator yoke and rotor yoke is uniform in all directions, which are μ_1 and μ_2.
5) The tooth and slots have different permeability in the r and θ directions, which are μ_1 and μ_θ.

Assumption 1) is to simplify the three-dimensional magnetic field into a two-dimensional magnetic field for the convenience of the solution. Assumption 2) represents the "real" stator winding, so that the solution is closer to the actual situation. Assumption 3) is the basic assumption commonly used in two-dimensional magnetic field analysis. Assumptions 4) and 5) reasonably consider the physical properties of different materials of the generator to make the solution closer to reality.

In Fig. 6, R_0 is the inside diameter of the rotor, R_{m2} is the inside diameter of the permanent magnet, R_{m1} is the
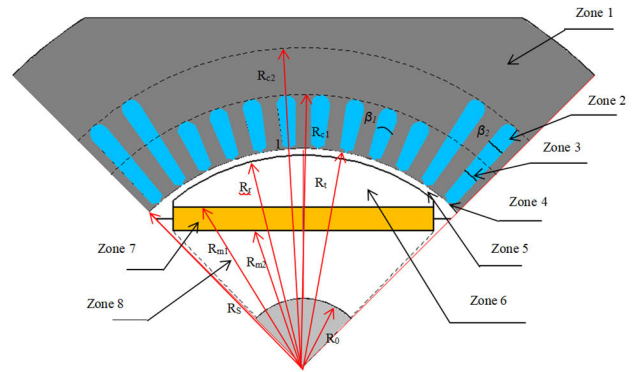
outside diameter of the permanent magnet, R_r is the radius of rotor pole, R_S is the radius of stator core, R_t is the radius of stator core slot-opening, R_{c1} is the slot position radius of three-phase stator winding, R_{c2} is the slot position radius of the single-phase stator winding.

Based on the basic structure and assumptions of STPDP-PMSG, a regional analytical model of the generator is established. Taking Fig. 6 as an example, the solution can be divided into stator yoke (Zone 1), stator slot: single-phase power stator winding (Zone 2), three-phase power stator winding (divided into upper and lower layers, Zone 3), stator slot-opening (Zone 4), air gap (Zone 5), magnetic metal block (Zone 6), rotor slot (Zone 7), rotor yoke (Zone 8).

Taking the center of slot 1 defined in Fig. 6 as the initial position, β_1 is the angle of the width of three-phase winding stator slot, β_2 is the angle of the width of single-phase winding stator slot, n_{S1} is the number of three-phase winding stator slots, n_{S2} is the number of single-phase winding stator slots, γ is the position angle between the initial slot containing the single-phase winding and the slot 1. The stator coordinates are based on the two-dimensional polar coordinate (r, θ) as the reference axis. Then the positions of the i-th slot of the three-phase winding and the j-th slot of the single-phase winding are defined as follows:

$$\theta_i = \frac{2\pi}{n_{S1}} (i - 1) \tag{2}$$

where $\theta_i \neq \theta_q$, $i = (1, 2, \cdots, 48)$.

$$\theta_q = \gamma + \frac{2\pi}{n_{S1}} (g + 12x) \tag{3}$$

where $g = (0, 1, 2, 3)$, $x = (0, 1, 2, 3)$.

In the same way, the center position of the j-th rotor of the permanent magnet can be defined as follows:

$$\theta_j = \frac{2\pi}{n_{S1}} (j - 1) + \Delta n_r \tag{4}$$

where δ is the angle of the width of rotor slot, n_r is the number of rotor slot number, Δn_r is the position of rotor angle. $x = (0, 1, 2, 3)$.

To facilitate the general solution of each subdomain model and the solution of harmonic coefficients, the authors define the following functions [17], [21]:

$$\begin{cases} P_x\left(y,z\right) = \left(\dfrac{y}{z}\right)^x + \left(\dfrac{z}{y}\right)^x \\ E_x\left(y,z\right) = \left(\dfrac{y}{z}\right)^x - \left(\dfrac{z}{y}\right)^x \end{cases} \tag{5}$$

D. THE GENERAL SOLUTION OF EACH SUBDOMAIN MODEL

The Laplace equation of the subdomain of stator yoke and boundary conditions are:

$$\frac{\partial^2 A_{11}}{\partial r^2} + \frac{1}{r}\frac{\partial A_{11}}{\partial r} + \frac{1}{r^2}\frac{\partial^2 A_{11}}{\partial \theta^2} = 0 \tag{6}$$

where $\theta \in \theta_i, R_S \le r \le R_1$.

$$\frac{\partial^2 A_{12}}{\partial r^2} + \frac{1}{r}\frac{\partial A_{12}}{\partial r} + \frac{1}{r^2}\frac{\partial^2 A_{12}}{\partial \theta^2} = 0 \tag{7}$$

where $\theta \in \theta_q, R_S \le r \le R_1$.

$$\begin{cases} A_{11i}|_{r=R_{c2}} = A_{2i}|_{r=R_{c2}} \\ \dfrac{1}{\mu_r}\dfrac{\partial A_{11i}}{\partial r}\bigg|_{r=R_{c2}} = \dfrac{1}{\mu_{\theta 1}}\dfrac{\partial A_{2i}}{\partial r}\bigg|_{r=R_{c2}} \\ A_{12i}|_{r=R_{c1}} = A_{3i}|_{r=R_{c1}} \\ \dfrac{1}{\mu_r}\dfrac{\partial A_{12i}}{\partial r}\bigg|_{r=R_{c1}} = \dfrac{1}{\mu_{\theta 1}}\dfrac{\partial A_{3i}}{\partial r}\bigg|_{r=R_{c1}} \end{cases} \tag{8}$$

According to the above boundary conditions, the general solution of the stator yoke subdomain is:

$$A_1\left(r,\theta\right)$$
$$= \sum_{k=1}^{\infty}\left[A_n^1\frac{R_S}{n}\frac{P_n\left(r,R_1\right)}{E_n\left(R_S,R_t\right)} + B_n^1\frac{R_t}{n}\frac{P_n\left(r,R_S\right)}{E_n\left(R_1,R_S\right)}\right]\cos\left(n\theta\right)$$
$$+ \sum_{n=1}^{\infty}\left[C_n^1\frac{R_S}{n}\frac{P_n\left(r,R_1\right)}{E_n\left(R_S,R_1\right)} + D_n^1\frac{R_t}{n}\frac{P_n\left(r,R_S\right)}{E_n\left(R_1,R_S\right)}\right]\sin\left(n\theta\right) \tag{9}$$

where A_n^1, B_n^1, C_n^1 and D_n^1 are the harmonic coefficients of the stator yoke subdomain.

The Poisson equation of the subdomain of stator slot and boundary conditions are:

$$\frac{\partial^2 A_1}{\partial r^2} + \frac{1}{r}\frac{\partial A_1}{\partial r} + \frac{1}{r^2}\frac{\partial^2 A_1}{\partial \theta^2} = -\mu J_3 \tag{10}$$

where $\theta_i - \frac{\alpha}{2} \le \theta \le \theta_i + \frac{\alpha}{2}, R_{C1} \le r \le R_{C2}$.

$$\begin{cases} A_{11i}|_{r=R_{c2}} = A_{2i}|_{r=R_{c2}} \\ \dfrac{1}{\mu_r}\dfrac{\partial A_{11i}}{\partial r}\bigg|_{r=R_{c2}} = \dfrac{1}{\mu_{\theta 1}}\dfrac{\partial A_{2i}}{\partial r}\bigg|_{r=R_{c2}} \\ A_{2i}|_{r=R_{c1}} = A_{3i}|_{r=R_{c1}} \\ \dfrac{\partial A_{2i}}{\partial r}\bigg|_{r=R_{c1}} = \dfrac{\partial A_{3i}}{\partial r}\bigg|_{r=R_{c1}} \end{cases} \tag{11}$$

$$\frac{\partial^2 A_2}{\partial r^2} + \frac{1}{r}\frac{\partial A_2}{\partial r} + \frac{1}{r^2}\frac{\partial^2 A_2}{\partial \theta^2} = -\mu\left(J_1 + J_2\right) \tag{12}$$

where $\theta_i - \frac{\alpha}{2} \le \theta \le \theta_i + \frac{\alpha}{2}, R_t \le r \le R_{C1}$.

$$\begin{cases} A_{12i}|_{r=R_{c2}} = A_{3i}|_{r=R_{c2}} \\ \dfrac{1}{\mu_r}\dfrac{\partial A_{12i}}{\partial r}\bigg|_{r=R_{c2}} = \dfrac{1}{\mu_{\theta 1}}\dfrac{\partial A_{3i}}{\partial r}\bigg|_{r=R_{c2}} \\ A_{3i}|_{r=R_{c1}} = A_{2i}|_{r=R_{c1}} \\ \dfrac{\partial A_{3i}}{\partial r}\bigg|_{r=R_{c1}} = \dfrac{\partial A_{2i}}{\partial r}\bigg|_{r=R_{c1}} \\ \dfrac{1}{\mu_{r2}}\dfrac{\partial A_{2i}}{\partial \theta}\bigg|_{\theta=\theta_i-\frac{\alpha}{2}} = \dfrac{1}{\mu_{r2}}\dfrac{\partial A_{3i}}{\partial \theta}\bigg|_{\theta=\theta_i+\frac{\alpha}{2}} = 0 \end{cases} \tag{13}$$

$$\frac{1}{\mu_{r2}}\frac{\partial A_{2i}}{\partial \theta}\bigg|_{\theta=\theta_i-\frac{\alpha}{2}} = \frac{1}{\mu_{r2}}\frac{\partial A_{3i}}{\partial \theta}\bigg|_{\theta=\theta_i+\frac{\alpha}{2}} = 0 \tag{14}$$

According to the method of separation of variables, combining (10)-(14), the general solution of the stator slot subdomain satisfying the boundary conditions are:

$$A_{2ig} = A_0^{2i} + B_0^{2i}\ln r + \sum_{n=1}^{\infty}\left[A_n^{2i}\frac{P_{\tau n}\left(r,R_{C2}\right)}{P_{\tau n}\left(R_{C1},R_{C2}\right)}\right.$$
$$\left. + B_n^{2i}\frac{P_{\tau n}\left(r,R_{C1}\right)}{P_{\tau n}\left(R_{C1},R_{C2}\right)}\right]\cos\left[\tau n\left(\theta+\frac{\alpha}{2}-\theta_i\right)\right] \tag{15}$$

$$A_{3ig} = A_0^{3i} + B_0^{3i}\ln r + \sum_{n=1}^{\infty}\left[A_n^{3i}\frac{P_{\tau n}\left(r,R_{C1}\right)}{P_{\tau n}\left(R_t,R_{C1}\right)}\right.$$
$$\left. + B_n^{3i}\frac{P_{\tau n}\left(r,R_t\right)}{P_{\tau n}\left(R_t,R_{C1}\right)}\right]\cos\left[\tau n\left(\theta+\frac{\alpha}{2}-\theta_i\right)\right] \tag{16}$$

where A_0^{2i}, B_0^{2i}, A_n^{2i} and B_n^{2i} are the harmonic coefficients of the subdomain of single-phase winding stator slot. A_0^{3i}, B_0^{3i}, A_n^{3i} and B_n^{3i} are the harmonic coefficients of the subdomain of three-phase winding stator slot.

The current density in the stator slot is mirrored by the left and right boundaries of the slot becomes a periodic signal whose period is b_{Sa1} [22]. The Fourier decomposition formula is as follows:

$$J_2 = J_{2i0} + \sum_{n=1}^{\infty}J_{2in}\cos\left[\tau_n\left(\theta+\frac{\alpha}{2}-\theta_i\right)\right] \tag{17}$$

where $J_{2i0} = \frac{1}{2\alpha}\int_{\theta_i-\frac{\alpha}{2}}^{\theta_i+\frac{3\alpha}{2}} J\left(\theta\right) d\theta = \frac{J_{21i}+J_{22i}}{2}$,

$$J_{2in} = \frac{1}{\alpha}\int_{\theta_i-\frac{\alpha}{2}}^{\theta_i+\frac{3\alpha}{2}} J\left(\theta\right)\cos\left[\tau_n\left(\theta+\frac{\alpha}{2}-\theta_i\right)\right]d\theta$$
$$= \frac{2\left(J_{21i}-J_{22i}\right)}{n\pi}\sin\left(\frac{n\pi}{2}\right).$$

$$J_3 = J_{3i0} + \sum_{n=1}^{\infty}J_{1in}\cos\left[\tau_n\left(\theta+\frac{\alpha}{2}-\theta_i\right)\right] \tag{18}$$

where $J_{3i0} = \frac{1}{2\alpha}\int_{\theta_i-\frac{\alpha}{2}}^{\theta_i+\frac{3\alpha}{2}} J\left(\theta\right) d\theta = \frac{J_{31i}+J_{32i}}{2}$,

$$J_{3in} = \frac{1}{\alpha}\int_{\theta_i-\frac{\alpha}{2}}^{\theta_i+\frac{3\alpha}{2}} J\left(\theta\right)\cos\left[\tau_n\left(\theta+\frac{\alpha}{2}-\theta_i\right)\right]d\theta$$

$$= \frac{2(J_{31i} - J_{32i})}{n\pi} \sin\left(\frac{n\pi}{2}\right).$$

$$J_4 = J_{4i0} + \sum_{n=1}^{\infty} J_{4in} \cos\left[\tau_n\left(\theta + \frac{\alpha}{2} - \theta_i\right)\right] \quad (19)$$

where $J_{4i0} = \frac{1}{2\alpha} \int_{\theta_i - \frac{\alpha}{2}}^{\theta_i + \frac{3\alpha}{2}} J(\theta)\, d\theta = \frac{J_{41i} + J_{42i}}{2}$,

$$J_{4in} = \frac{1}{\alpha} \int_{\theta_i - \frac{\alpha}{2}}^{\theta_i + \frac{3\alpha}{2}} J(\theta) \cos\left[\tau_n\left(\theta + \frac{\alpha}{2} - \theta_i\right)\right] d\theta$$

$$= \frac{2(J_{41i} - J_{42i})}{n\pi} \sin\left(\frac{n\pi}{2}\right).$$

the particular solutions obtained from the above analysis are:

$$A_{3ip} = -\frac{\mu_0}{4} J_{3i0} r^2 + \sum_{n=1}^{\infty} \frac{\mu_0 J_{3in}}{\tau_n^2 - 4} r^2 \cos\left[\theta + \frac{\alpha}{2} - \theta_i\right] \quad (20)$$

$$A_{4ip} = -\frac{\mu_0}{4}(J_{4i0} + J_{4i0}) r^2 + \sum_{n=1}^{\infty} \frac{\mu_0 (J_{41in} + J_{42in})}{\tau_n^2 - 4} r^2$$

$$\times \cos\left[\theta + \frac{\alpha}{2} - \theta_i\right] \quad (21)$$

The general solutions are:

$$A_2(r, \theta) = A_{2g} + A_{2ip} \quad (22)$$

$$A_3(r, \theta) = A_{3g} + A_{3ip} \quad (23)$$

The Poisson equation of the subdomain of PM and boundary conditions are:

$$\frac{\partial^2 A_7}{\partial r^2} + \frac{1}{r}\frac{\partial A_7}{\partial r} + \frac{1}{r^2}\frac{\partial^2 A_7}{\partial \theta^2} = -\frac{\mu_0}{r}\left(M_{j\theta} - \frac{\partial M_{jr}}{\partial \theta}\right) \quad (24)$$

where $\theta_j - \frac{\delta}{2} \le \theta \le \theta_j + \frac{\delta}{2}, R_{m1} \le r \le R_{m2}$.

$$\begin{cases} A_{7i}|_{r=R_{m1}} = A_{6i}|_{r=R_{m1}} \\ \frac{1}{\mu_{\theta 2}}\frac{\partial A_{7i}}{\partial r}\bigg|_{r=R_{m1}} = \frac{1}{\mu_r}\frac{\partial A_{6i}}{\partial r}\bigg|_{r=R_{m1}} \\ A_{7i}|_{r=R_{m2}} = A_{6i}|_{r=R_{m2}} \\ \frac{1}{\mu_r}\frac{\partial A_{8i}}{\partial r}\bigg|_{r=R_{m2}} = \frac{1}{\mu_{\theta 2}}\frac{\partial A_{7i}}{\partial r}\bigg|_{r=R_{m2}} \end{cases} \quad (25)$$

where M_{jr} is the radial component of the remanent magnetization of the j-th permanent magnet; $M_{j\theta}$ is the tangential component of the remanent magnetization of the j-th permanent magnet.

The solution process of the rotor slot subdomain is similar to the solution process of the stator slot. In this way, after mirroring the permanent magnets in the rotor slot, a periodic signal whose period 2δ is formed.

Carry out Fourier series expansion on the radial and tangential components of the magnetization of the j-th permanent magnet in a period after the mirror image, which can be expressed as:

$$\begin{cases} M_{jr} = C_7 \sum_{n=1,2,3,\cdots}^{\infty} M_{rn} \sin\left[\tau_n\left(\theta + \frac{\delta}{2} - \theta_j\right)\right] \\ M_{j\theta} = C_7 \sum_{n=1,2,3,\cdots}^{\infty} M_{\theta n} \cos\left[\tau_n\left(\theta + \frac{\delta}{2} - \theta_j\right)\right] \end{cases} \quad (26)$$

Therefore, the general solutions of the rotor slot subdomain satisfying the boundary conditions are:

$$A_{7j}(r, \theta)$$

$$= A_0^{7j} + B_0^{7j} \ln r + \sum_{n=1}^{\infty} \left[A_n^{7j} \frac{P_{\tau n}(r, R_{m2})}{P_{\tau n}(R_{m1}, R_{m2})}\right.$$

$$\left. + B_n^{7j} \frac{P_{\tau n}(r, R_{m1})}{P_{\tau n}(R_{m2}, R_{m1})}\right] \cos\left[\tau n\left(\theta + \frac{\delta}{2} - \theta_j\right)\right] + A_{7jp} \quad (27)$$

where A_0^{7j}, B_0^{7j}, A_n^{7j} and B_n^{7j} are the harmonic coefficients of the rotor slot subdomain.

$$f_{jn}(r) = \begin{cases} C_7\left(-\mu_0 \frac{\tau_n M_{rn} - M_{\theta n}}{\tau_n^2 - 1} r\right), & \tau_n \ne 1 \\ C_7\left(\mu_0 \frac{\tau_n M_{rn} - M_{\theta n}}{2} r \ln r\right), & \tau_n = 1 \end{cases} \quad (28)$$

The Laplace equation and its general and special solution of other parts of STPDP-PMSG can be solved by the above method, so the authors will not repeat it here.

E. BASIC PRINCIPLES OF FINITE ELEMENT ANALYSIS

Finite element method (FEM) solves discrete elements separately by dividing a continuous complex field in engineering into finite elements. Under the premise of considering the initial value conditions and boundaries of the calculation, the final result can be obtained by adding all the solving elements.

For the solution of STPDP-PMSG electromagnetic field, the Maxwell equations in integral form are converted into differential form to solve the electromagnetic field. The expression is as follows:

$$\begin{cases} \nabla \times \vec{H} = \vec{J} + \frac{\partial \vec{D}}{\partial t} \\ \nabla \times \vec{B} = -\frac{\partial \vec{B}}{\partial t} \\ \nabla \cdot \vec{D} = \rho \\ \nabla \cdot D = 0 \end{cases} \quad (29)$$

where $\vec{D}$ is an electric displacement vector, $\vec{H}$ is the magnetic field intensity, $\vec{B}$ is magnetic flux density, $\vec{J}$ is current density, ρ is resistivity.

IV. VERIFICATION OF FINITE ELEMENT SIMULATION

The authors take a 4-pole 48-slot STPDP-PMSG as an example to verify the analytical model by two-dimensional finite element simulation.

A. NO-LOAD AIR GAP FLUX DENSITY

According to the relationship between the magnetic flux density and the magnetic vector potential, The mathematical expressions of the radial and tangential components of the air gap flux density (B_{4rj} and $B_{4\theta j}$) generated by the j-th

permanent magnet can be obtained, which are:

$$
\begin{cases}
B_{4rj} = \sum_y y\left[\dfrac{A_y^4}{R_s}\left(\dfrac{r}{R_s}\right)^{y-1} + \dfrac{B_y^4}{R_r}\left(\dfrac{r}{R_r}\right)^{-y-1}\right]\sin(y\theta) \\
\quad + \sum_y y\left[\dfrac{C_y^4}{R_s}\left(\dfrac{r}{R_s}\right)^{k-1} + \dfrac{D_y^4}{R_r}\left(\dfrac{r}{R_r}\right)^{-k-1}\right]\cos(y\theta) \\[2mm]
B_{4\theta j} = -\sum_y y\left[\dfrac{A_y^4}{R_s}\left(\dfrac{r}{R_s}\right)^{y-1} + \dfrac{B_y^4}{R_r}\left(\dfrac{r}{R_r}\right)^{-y-1}\right]\cos(y\theta) \\
\quad - \sum_y y\left[\dfrac{C_y^4}{R_s}\left(\dfrac{r}{R_s}\right)^{k-1} - \dfrac{D_y^4}{R_r}\left(\dfrac{r}{R_r}\right)^{-k-1}\right]\sin(y\theta)
\end{cases}
$$

$$(30)$$

Then the radial and tangential air gap flux density considering the effect of slotting is:

$$
\begin{cases}
B_{4r} = \lambda_g(r,\theta)\sum_y B_{4rj} \\
B_{4\theta} = \lambda_g(r,\theta)\sum_y B_{4\theta j}
\end{cases}
$$

$$(31)$$

Fig.7 shows the comparison of the radial air gap flux density waveform calculated by ANA and FEM. It can be seen that the analytical results of ANA are in good agreement with the FEM; the radial effective values are 9.1101T and 9.6748T, respectively; the error of the two methods is 6.2%. The analytical result of the nonlinear subdomain method is slightly higher than the result of FEM because the end effect of the generator is ignored when using the subdomain analytical method.

B. NO-LOAD BEMF

Assuming that the windings in the stator slots are uniformly distributed, based on Stokes' theorem, at any rotor position, according to the relationship between the flux linkage and the magnetic vector position, the flux linkage generated by the windings in the *i*-th slot can be obtained. The flux linkage expressions are:

$$
\begin{cases}
\psi_{i3} = \dfrac{L_{ef}N_{c3}}{S_3}\displaystyle\int_{R_{C1}}^{R_{C2}}\int_{\theta_i-\frac{\alpha}{2}}^{\theta_i+\frac{\alpha}{2}} A_{3i}\,r\,dr\,d\theta \\
\psi_{i1} = \dfrac{L_{ef}N_{c1}}{S_1}\displaystyle\int_{R_t}^{R_t+h_1}\int_{\theta_i-\frac{\alpha}{2}}^{\theta_i+\frac{\alpha}{2}} A_{1i}\,r\,dr\,d\theta \\
\psi_{i2} = \dfrac{L_{ef}N_{c1}}{S_2}\displaystyle\int_{R_t+h_1}^{R_{c1}}\int_{\theta_i-\frac{\alpha}{2}}^{\theta_i+\frac{\alpha}{2}} A_{2i}\,r\,dr\,d\theta
\end{cases}
$$

$$(32)$$

$$
\begin{cases}
S_3 = \dfrac{\alpha\left(R_{c2}^2 - R_{c1}^2\right)}{4} \\
S_2 = \dfrac{\alpha\left(R_{c1}^2 - R_{t1}^2\right)}{4} \\
S_1 = \dfrac{\alpha\left(R_{t1}^2 - R_t^2\right)}{4}
\end{cases}
$$

$$(33)$$

where, L_{ef} is the axial length of the generator, N_{c3} is the number of turns of single-phase coil, N_{c1} is the number of turns of three-phase coil, S is the sectional area of winding.
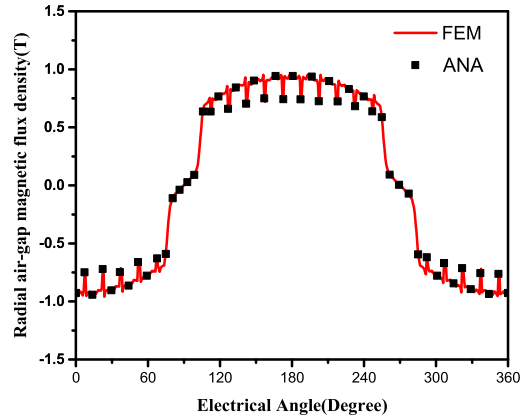

FIGURE 7. Comparison of radial air gap flux density waveform.

Taking the prototype designed in this study as an example, according to the distribution of three-phase winding coils and single-phase winding coils in the stator slots, the following definitions are as follows:

$$
\begin{cases}
C_A = [C_{cellA}\cdots C_{cellA}]_{1\times 2} \\
C_B = [C_{cellB}\cdots C_{cellB}]_{1\times 2} \\
C_C = [C_{cellC}\cdots C_{cellC}]_{1\times 2} \\
C_D = [C_{cellD}\cdots C_{cellD}]_{1\times 2}
\end{cases}
$$

$$(34)$$

where C_{cell} is the distribution matrix of the coil in a certain phase and a pole-phase group.

Then:

$$
\begin{cases}
\varphi_A = C_A\psi_A \\
\varphi_B = C_B\psi_B \\
\varphi_C = C_C\psi_C \\
\varphi_D = C_D\psi_D
\end{cases}
$$

$$(35)$$

$$
\begin{cases}
e_A = -\dfrac{d\varphi_A}{dt} = -\dfrac{d\varphi_A}{d\theta}\dfrac{d\theta}{dt} = -\omega_r\dfrac{d\varphi_A}{d\theta} \\
e_B = -\dfrac{d\varphi_B}{dt} = -\dfrac{d\varphi_B}{d\theta}\dfrac{d\theta}{dt} = -\omega_r\dfrac{d\varphi_B}{d\theta} \\
e_C = -\dfrac{d\varphi_C}{dt} = -\dfrac{d\varphi_C}{d\theta}\dfrac{d\theta}{dt} = -\omega_r\dfrac{d\varphi_C}{d\theta} \\
e_D = -\dfrac{d\varphi_D}{dt} = -\dfrac{d\varphi_D}{d\theta}\dfrac{d\theta}{dt} = -\omega_r\dfrac{d\varphi_D}{d\theta}
\end{cases}
$$

$$(36)$$

Fig.8 shows the comparison of no-load line BEMF waveform of three-phase port in half a cycle obtained by ANA and FEM. The effective values are 417.6V and 411.78V respectively. Fig.9 shows the comparison of the no-load phase BEMF waveform of single-phase port in half a cycle obtained by the two methods. The effective values are 244.6V and 239.5V respectively.

As can be seen from Table 3, the calculation error of the two methods for the no-load line BEMF of the three-phase port in half a cycle is 1.03%. The calculation error of single-phase port no-load line BEMF in half a cycle is 1.24%. It can be seen that the calculated values of the two calculation methods are very close.
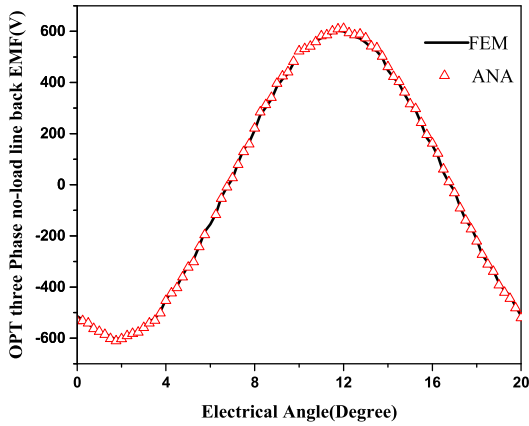
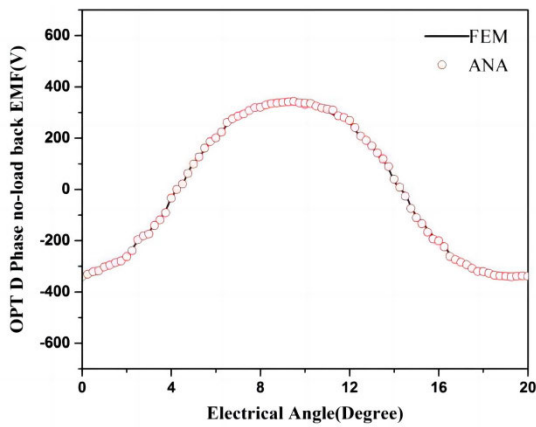**FIGURE 8.** Comparison of the no-load line BEMF waveform of three-phase port.

FIGURE 9. Comparison of the no-load phase BEMF waveform of single-phase port.

TABLE 3. Comparison of error between simulation results and experimental results.

Method	Port BEMF	Calculated value /V	Relative error /%
FEM	no-load line BEMF of three-phase port	417.8	0
	no-load phase BEMF of single-phase port	244.7	0
ANA	no-load line BEMF of three-phase port	413.6	1.03
	no-load phase BEMF of single-phase port	241.3	1.24

V. EXPERIMENTAL VERIFICATION

To verify the accuracy of nonlinear subdomain method, the authors design and manufacture a 4-pole 48-slot STPDP-PMSG with eccentric magnetic metal block structure. The no-load experiments are carried out on the manufactured prototype to measure the three-phase port line BEMF and single-phase port phase BEMF. The experimental test platform is shown in Fig.10. During the experiment, the STPDP-PMSG is connected to an prime motor through a coupling and the no-load test is performed at rated speed.
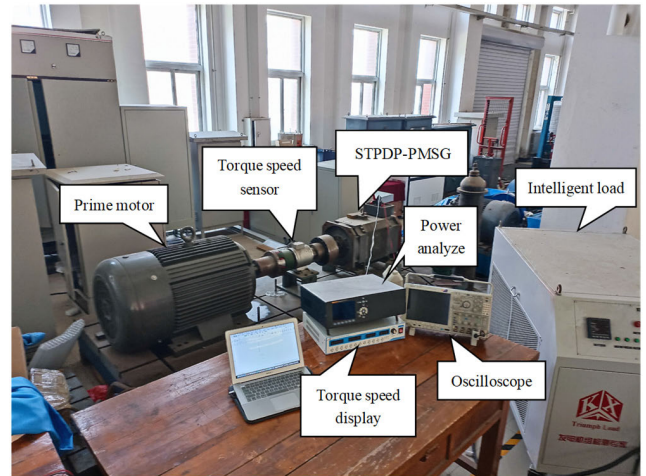

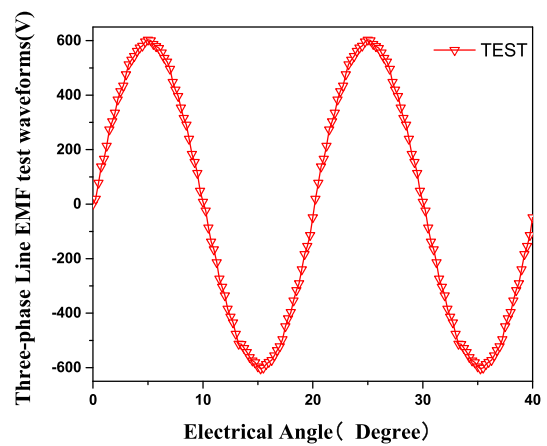**FIGURE 10.** Experimental test platform of STPDP-PMSG.

FIGURE 11. The experimental waveform of the no-load line BEMF waveform of three-phase port.
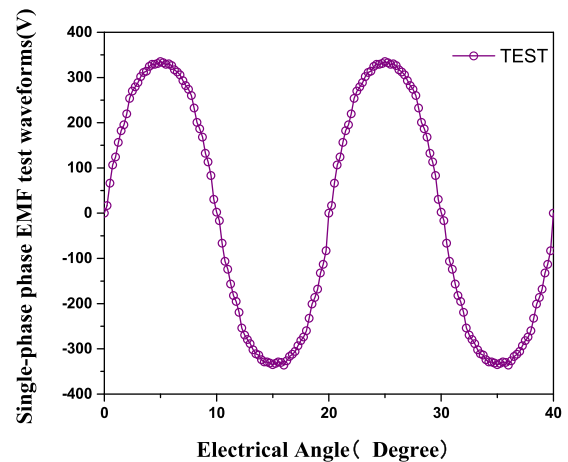

FIGURE 12. The experimental waveform of the no-load phase BEMF waveform of single-phase port.

Fig.11 shows the experimentally measured no-load line BEMF waveform of three-phase port; the effective value is

TABLE 4. Comparison of voltage experimental values, FEM calculated values and ANA calculated values of STPDP-PMSG two ports.

BEMF	Method	Calculated value/V	Relative error/%
no-load line BEMF of three-phase port	Experimental values	404.3	0
	FEM	417.8	3.4
	ANA	413.6	2.3
no-load phase BEMF of single-phase port	Experimental values	236.7	0
	FEM	244.7	3.4
	ANA	241.3	1.9

404.3V. Fig.12 shows the experimentally measured no-load phase BEMF waveform of single-phase port; the effective value is 236.7V.

Combining Table 3 and comparing Figures 11 and 12, a comparative table of the relative errors of ANA and FEM analysis results relative to experimental results can be obtained, as shown in Table 4.

As shown in Table 4, compared with the experimental test results, the error values of the three-phase line BEMF and the single-phase port BEMF calculated by the ANA are 2.3% and 1.9%; the error values of the three-phase line BEMF and the single-phase port BEMF calculated by the FEM are 3.4% and 3.4%.

It can be seen that for the special stator structure of STPDP-PMSG, the error value calculated by ANA is smaller than the error value of FEM, thus verifying the correctness and effectiveness of the ANA method in this paper.

VI. CONCLUSION

For the permanent synchronous magnet generator with separate three-phase port and single-phase port structure, the authors have proposed a magnetic field analytical method of nonlinear subdomain model to obtain an accurate magnetic field model of STPDP-PMSG. This method solves the magnetic reluctance problem of stator and rotor materials which is usually ignored in traditional analytical methods. It can describe the electromagnetic parameters of STPDP-PMSG more accurately and provide necessary reference for the design of STPDP-PMSG. Compared with the finite element simulation calculation results, the radial air gap flux density and no-load BEMF waveform of STPDP-PMSG port calculated by the nonlinear subdomain method are in good agreement, and the calculation error of the effective value is low.

Meanwhile, the authors have used genetic algorithm to optimize the design of the eccentric structure model of the magnetic metal block of STPDP-PMSG.The optimization results show that the distortion rate of the air gap flux density waveform and the BEMF waveform of the two ports are all effectively suppressed.

Based on this, a prototype has been manufactured and tested by the authors. The test results of the no-load BEMF of the two ports of the generator are in good agreement with the results obtained by the nonlinear subdomain model, which verifies the accuracy and effectiveness of the analytical method.

REFERENCES

[1] L. J. Wu, Z. Q. Zhu, D. Staton, M. Popescu, and D. Hawkins, "Analytical model of eddy current loss in windings of permanent-magnet machines accounting for load," *IEEE Trans. Magn.*, vol. 48, no. 7, pp. 2138–2151, Jul. 2012.

[2] D. Golovanov and C. Gerada, "An analytical subdomain model for dual-rotor permanent magnet motor with Halbach array," *IEEE Trans. Magn.*, vol. 55, no. 12, pp. 1–4, Dec. 2019.

[3] L. Xu, Q. B. Wu, and X. Gong, "Network-varying equivalent magnetic circuit modeling of novel disk transverse-flux permanent magnet brushless machine," *Trans. China Electro-Tech. Soc.*, vol. 31, no. 17, pp. 147–153, 2016.

[4] W. Yang, Z. X. Deng, and H. S. Zhang, "Exact analytical solution of magnetic field in permanent magnet in-wheel motor," *Trans. China Electro-Tech. Soc.*, vol. 34, no. 7, pp. 1423–1433, 2019.

[5] Z. Q. Zhu, L. J. Wu, and Z. P. Xia, "An accurate subdomain model for magnetic field computation in slotted surface-mounted permanent-magnet machines," *IEEE Trans. Magn.*, vol. 46, no. 4, pp. 1100–1115, Apr. 2010.

[6] L. J. Wu, Z. Q. Zhu, D. Staton, M. Popescu, and D. Hawkins, "An improved subdomain model for predicting magnetic field of surface-mounted permanent magnet machines accounting for tooth-tips," *IEEE Trans. Magn.*, vol. 47, no. 6, pp. 1693–1704, Jun. 2011.

[7] Y. X. Sun, C. T. Chen, and X. Q. Zheng, "Calculation of suspension force of amorphous alloy high-speed maglev linear motor based on distributed magnetic circuit method," *Trans. China Electro-Tech. Soc.*, p. 38, 2023.

[8] G. C. Pang, Z. Q. Deng, and Z. M. Zhang, "Analytical calculation of no-load air gap magnetic field in surface-mounted permanent magnet motor based on improved generalized magnetic circuit method," *Trans. China Electro-Tech. Soc.*, vol. 34, no. 22, pp. 4623–4633, 2019.

[9] J. Li, L. Jing, X. Y. Zhou, and Y. Zhang, "Exact analytical method for surface-mounted permanent magnet brushless motors," *Trans. China Electro-Tech. Soc.*, vol. 27, no. 11, pp. 83–88, 2012.

[10] Z. H. Zhang, Q. K. Han, and X. P. Xu, "Air gap magnetic field calculation of permanent magnet direct drive generator based on conformal mapping and magnetic equivalent circuit method," *Trans. China Electro-Tech. Soc.*, vol. 38, no. 3, pp. 703–711, 2023.

[11] Z. J. Qiu, C. Li, and X. Y. Zhou, "Analytical calculation of no-load air-gap magnetic field in surface-mounted permanent magnet motors with rotor eccentricity," *Trans. China Electro-Tech. Soc.*, vol. 28, no. 3, pp. 114–121, 2013.

[12] Y. Zhou, H. Li, G. Meng, S. Zhou, and Q. Cao, "Analytical calculation of magnetic field and cogging torque in surface-mounted permanent-magnet machines accounting for any eccentric rotor shape," *IEEE Trans. Ind. Electron.*, vol. 62, no. 6, pp. 3438–3447, Jun. 2015.

[13] M. Baghayipour, A. Darabi, and A. Dastfan, "An analytical model of harmonic content no-load magnetic fields and back EMF in axial flux PM machines regarding the iron saturation and winding distribution," *COMPEL-Int. J. Comput. Math. Electr. Electron. Eng.*, vol. 37, no. 1, pp. 54–76, Jan. 2018.

[14] S. S. Zhang and S. Y. Guo, "Analytical magnetic field method of permanent magnet synchronous machine considering step-skewed magnets and magnetic slot wedge," *Trans. China Electro-Tech. Soc.*, vol. 34, no. 1, pp. 15–26, 2019.

[15] S. Li, Y. J. Zhang, and L. B. Jing, "Researches on exact analytical method of Halbach-array permanent magnet motors with semi-closed slots," *Proc. CSEE*, vol. 33, no. 33, pp. 85–94, 2013.

[16] J. J. Fan, J. H. Wu, and C. P. Li, "Solution of permanent magnet synchronous motors with partition between poles Halbach magnet," *Trans. China Electro-Tech. Soc.*, vol. 28, no. 3, pp. 36–42, 2013.

[17] S. Guo and L. Zhou, "Analytical solution of magnetic field in surface-inset permanent magnet machines," *Proc. CSEE*, vol. 35, no. 3, pp. 710–718, Mar. 2014.

[18] H. C. Li, L. Y. Li, and J. K. Yu, "Analytic calculation of no-load air-gap magnetic fields of polygonal rotor magnetic yoke permanent magnet synchronous motors," *Proc. CSEE*, vol. 38, no. 5, pp. 3354–3364, 2018.

[19] G. F. Uler, O. A. Mohammed, and C.-S. Koh, "Utilizing genetic algorithms for the optimal design of electromagnetic devices," *IEEE Trans. Magn.*, vol. 30, no. 6, pp. 4296–4298, Nov. 1994.

[20] R. Akinci and M. Polat, "Design and optimization with genetic algorithm of double rotor axial flux permanent magnet synchronous motor (TORUS type) for electrical vehicles," in *Proc. 4th Int. Conf. Power Electron. Their Appl. (ICPEA)*, Sep. 2019, pp. 1–5.

[21] T. Lubin, S. Mezani, and A. Rezzoug, "2-D exact analytical model for surface-mounted permanent-magnet motors with semi-closed slots," *IEEE Trans. Magn.*, vol. 47, no. 2, pp. 479–492, Feb. 2011.

[22] B. L. J. Gysen, K. J. Meessen, J. J. H. Paulides, and E. A. Lomonova, "General formulation of the electromagnetic field distribution in machines and devices using Fourier analysis," *IEEE Trans. Magn.*, vol. 46, no. 1, pp. 39–52, Jan. 2010.

GUIHONG FENG received the B.S. degree in electrical engineering from the Shenyang University of Technology, Shenyang, China, in 1985, and the M.S. degree in electric drive and automation from Northeastern University, Shenyang, in 1994. She is currently a Professor with the Shenyang University of Technology. Her research interests include design and optimization of electrical machines, low speed high torque drive systems, and power system automation.

KAI LI received the B.S. and M.S. degrees in electrical engineering and automation from the Shenyang University of Technology, Shenyang, China, in 2012, where he is currently pursuing the Ph.D. degree in electrical engineering. His research interests include design and control of permanent magnet motor, special electrical machine with its control, and direct drive system of permanent magnet motor.

BINGYI ZHANG received the B.S., M.S., and Ph.D. degrees in electrical engineering from the Shenyang University of Technology, Shenyang, China, in 1982, 1987, and 2007, respectively. He is currently a Professor with the Shenyang University of Technology. His research interests include design and optimization of electrical machines, low speed high torque drive systems, and power system automation.

KAI LIU received the B.S. degree in electrical engineering and automation from the Shenyang University of Technology, Shenyang, China, in 2013, where he is currently pursuing the Ph.D. degree in electric machines and electric apparatus. His research interests include special electrical machine with its control and direct drive system of permanent magnet motor.

● ● ●